Vol. 3(Iss. 1) 2026, pp.213-237, African Scientific Annual Review www.asarev.net ISSN: 3007-0902

Mathematical modeling of the effect of rainfall variation on cholera transmission dynamics

[1*]Simon Wekesa Simiyu
[2]Frankline Tireito
[3]Colleta Akinyi

[1,2,3] Department of Mathematics, Masinde Muliro University of Science and Technology, Kakamega, Kenya.

[1*] simiyusimon20@gmail.com

https://doi.org/10.51867/asarev.maths.3.1.20

Abstract

Cholera remains a major public health challenge, particularly in regions with inadequate access to safe water and sanitation. Rainfall variation has been associated with recurrent cholera outbreaks, with both heavy rainfall and drought increasing disease transmission through distinct environmental mechanisms. This study developed and analyzed a nonlinear rainfall-dependent SIR-B mathematical model to assess the effect of rainfall variation on cholera transmission dynamics. A rainfall parameter was incorporated to capture the increased transmission associated with flooding and drought. The model was shown to be well-posed through positivity and boundedness analyses, while the disease-free and endemic equilibrium points and their local stability were established. Under the rainfall conditions considered, the basic reproduction number satisfied $R_0 > 1$, implying an unstable disease-free equilibrium and a locally asymptotically stable endemic equilibrium. Numerical simulations performed demonstrated that heavy rainfall produced the highest infection levels and environmental pathogen concentration, moderate rainfall resulted in the lowest transmission potential, while drought exhibited an intermediate disease burden. The findings further revealed that environmental transmission contributed more substantially to the overall transmission potential than direct human-to-human transmission, confirming that rainfall variation primarily influences cholera dynamics through the environmental pathway. Generally, the proposed rainfall-dependent SIR-B model provides valuable insights into the role of rainfall variation in cholera transmission and may support the design of effective water, sanitation, hygiene, and environmental management strategies, particularly during periods of heavy rainfall and drought.

MSC2010 Subject Classification: 92D30; 34A26; 37N25
Keywords: Cholera; mathematical modelling; rainfall variation; transmission dynamics; SIR-B model; basic reproduction number.

1 Introduction

Cholera is an acute *diarrhoeal* infection caused by bacterium *Vibrio cholerae* of serogroup 01 and 0139. The disease is transmitted through ingestion of contaminated food and water [21]. The transmission and persistence of cholera are influenced by several environmental and socioeconomic factors, including access to safe drinking water, sanitation, hygiene practices, population density and climatic conditions [16]. Among these factors, rainfall has received considerable attention because it

Licensed Under Creative Commons Attribution (CC BY-NC)

directly affects the quality, availability and contamination of water sources, thereby influencing the survival and transmission of *Vibrio cholerae* [7, 19, 24]. Although WHO mentions poverty and conflict as the main drivers of disease transmission [1], cholera outbreak frequency is closely linked to climatic changes. These relationships have implications for cholera outbreaks [4, 24]. Variation in the climate is likely to lead to changes in the frequency of rainfall events [15].

Variations in rainfall, including excessive rainfall and prolonged drought, alter environmental conditions that favour the survival and transmission of *Vibrio cholerae*. Excessive rainfall often leads to flooding and contamination of drinking water sources, whereas prolonged drought reduces access to safe water and increases reliance on contaminated water sources, thereby increasing the risk of cholera transmission [7, 12, 22]. Several links between both extremely high rainfall and low rainfall and cholera incidences have been described in Africa, where half of the world's reported cholera cases are in Sub-Saharan Africa with the highest fatality rates [12, 18].

Koelle[10] developed an S-I-R model on the impact of the climate on the disease dynamics of cholera. The two main objectives for the study were; reconstruction of the immunity patterns and population sizes; identification of the respective roles of extrinsic and intrinsic factors in the disease dynamics. The model specifically examined how climate variability influences the transmutability of cholera impacting outbreak size and incidences. The disease dynamics was modeled with different equations.

Although this model shows climatic variations as one of the agents of cholera disease outbreak, however, it has the following challenges; the absence of an environmental pathogen compartment and the fact that rainfall is not an explicit variable make it difficult to formulate a direct rainfall-effect model or conduct a mechanistic examination of how rainfall variation affects system stability. In addition, the existing model does not give the quantitative data of the effect of rainfall variation on the dynamics of cholera.

Codeco[5] developed an S-I-B mathematical model of cholera epidemiology incorporating environmental reservoir of *vibro cholerae*. The aim of their study was to explore the role of the aquatic reservoir on the persistence of endemic and secondly to find the minimum conditions for the development of the endemic and epidemic cholera. The mathematical equations for Codeco's model are as follows;

$$\begin{aligned} \frac{dS}{dt} &= n(H - S) - a\lambda(B)S \\ \frac{dI}{dt} &= a\lambda(B)S - rI \\ \frac{dB}{dt} &= B(nb - mb) + eI \end{aligned} \tag{1}$$

While Codeco provided a pioneering framework by establishing the aquatic reservoir as an active driver of cholera dynamics, the model has several limitations; It excludes human-to-human transmission, considering only environmental transmission, which underestimates transmission in settings where direct contact is important. Although Codeco acknowledges seasonal variation, the model does not identify the underlying climatic drivers, limiting its utility for understanding how rainfall affects transmission. The absence of a recovered compartment prevents the model from tracking immunity dynamics and re-infection. The model lacks a formal sensitivity analysis to identify key intervention

Licensed Under Creative Commons Attribution (CC BY-NC)

targets. The model does not incorporate the effects of climate variability, particularly rainfall, on pathogen dynamics. These limitations underscore the need for a more comprehensive framework that captures the full complexity of cholera transmission under varying climatic conditions.

Zhou and Cui[27] developed a mathematical model to investigate how seasonal environmental variations influence cholera transmission dynamics. The authors extended classical SIR cholera models by incorporating periodic transmission rates that capture the seasonal nature of cholera outbreaks observed in many endemic regions. While the model provides valuable insights into seasonally driven cholera dynamics, it presents the following limitations; the transmission rates are assumed to follow a fixed sinusoidal pattern, which does not account for the irregular and extreme rainfall events such as flooding and prolonged drought that increasingly characterize climate variability. In addition the environmental transmission rate depends solely on periodic time functions rather than on explicit hydrological or climatic drivers, limiting the model's ability to capture the nonlinear effects of rainfall extremes on water contamination and availability. The model also does not distinguish between the contrasting mechanisms through which excessive rainfall and drought influence transmission, treating both simply as seasonal variations in transmission intensity.

Asadgol and Mohammadi[2] developed a model on the effect of the climate change on cholera diseases dynamics using Artificial Neural Networks (ANNs) to estimate the future trend of cholera incidence from the year 2021 to 2050 in Qom city. The results of the model showed that there is a strong correlation between both precipitation or high temperature and subsequent increases in cholera incidences, providing robust empirical evidence that both low precipitation and high temperature in warmer months could enhance the swifter bacterial replication. It also showed that the future climate in Qom City could be warmer and wetter by the year 2050, which could increase cholera cases under a worse scenario with the highest number of cases being recorded in warmer months. Although this model could establish the link between climate drivers and cholera dynamics directly,however, the model gives only correlative data on how rainfall variation affects the dynamics of cholera. There was lack of nonlinear epidemiological model capable of quantifying how variations in rainfall intensity and timing directly influence cholera dynamics.

Mukandavire and Liao [13] formulated a compartmental model to estimate the reproductive numbers for the 2008–2009 cholera outbreaks in Zimbabwe. The model incorporated both human-to-human and environment-to-human transmission pathways, providing critical estimates for the environmental transmission rate β. Their study demonstrated that the environmental reservoir plays a significant role in sustaining cholera epidemics, with implications for understanding how rainfall variation affects pathogen persistence. Nevertheless, the study did not account for seasonal or climatic forcing of transmission parameters. The environmental transmission rate was treated as constant throughout the outbreak period, failing to capture the temporal variability induced by rainfall events, which is a central focus of the current research.

The synthesis reveals a consistent limitation. While models like [5, 27] provide the necessary environmental structure and [2, 10] establish the climate link, none integrate a direct functional relationship where a rainfall parameter dynamically modulates the cholera transmission through the environmental transmission pathway. This research directly addresses these gaps by: Formulating an S-I-R-B model where the net growth rate of *Vibrio cholerae* is a function of a rainfall parameter. Performing stability using the basic reproduction number $\mathcal{R}_0$ by proving the existence of disease free and endemic

Licensed Under Creative Commons Attribution (CC BY-NC)

equilibrium, and illustrating graphically through simulation how varying rainfall parameters push the system across epidemic thresholds, providing a quantitative tool for climate-informed outbreak forecasting and intervention planning.

2 Model Formulation and Analysis

2.1 Model formulation

In this model, the total human population at time t, denoted $N(t)$, is divided into three epidemiological compartments: susceptible individuals $S(t)$, infected individuals $I(t)$, and recovered individuals $R(t)$. The model also tracks the concentration of *Vibrio cholerae* in the environment, $B(t)$. The susceptible population is replenished through births and immigration. All human compartments experience natural death at rate μ, with infected individuals additionally facing disease-induced death at rate γ.

Cholera transmission occurs via two pathways: direct human-to-human transmission at rate α, and environment-to-human transmission at rate $\beta(\theta)$, with the force of infection given by:

$$\psi = \alpha I + \frac{\beta(\theta)B}{\kappa + B},$$

where $\frac{B}{\kappa+B}$ is the probability of the susceptible individual to acquire infection from environmental exposure, and κ is the half-saturation constant. A central feature of the model is the rainfall variation parameter $\theta \in [0, 1]$, which is incorporated into the environmental transmission component to explicitly account for the influence of rainfall on cholera transmission.

Rainfall modifies the efficiency with which environmental bacteria infect susceptible individuals through the rainfall-dependent transmission coefficient

$$\beta(\theta) = \beta_1(1-\theta)^2 + \beta_2\theta^2, \qquad 0 \le \theta \le 1, \tag{2}$$

where β_1 and β_2 denote the environmental transmission rates during heavy rainfall and drought, respectively, with $\beta_1 > \beta_2$. The quadratic form is adopted as a simplified representation of the nonlinear relationship between rainfall variation and environmental cholera transmission. It captures the possibility that both rainfall extremes can increase transmission through different environmental mechanisms, while intermediate rainfall conditions are associated with lower transmission. During heavy rainfall ($\theta \to 0$), flooding promotes widespread contamination of drinking water by dispersing *Vibrio cholerae* from sewage and other environmental reservoirs. Conversely, during drought ($\theta \to 1$), reduced availability of safe water forces communities to rely on contaminated water sources, thereby increasing exposure to the pathogen.

Infected individuals recover naturally at rate ξ and move to the recovered compartment. Recovered individuals may lose immunity at rate δ, after which they re-enter the susceptible compartment. Pathogen dynamics include intrinsic growth at rate ρ, shedding from infected individuals at rate ω, and natural decay at rate ϵ. The concentration of *Vibrio cholerae* in the environment evolves according to:

$$\frac{dB}{dt} = \rho B + \omega I - \epsilon B,$$

Licensed Under Creative Commons Attribution (CC BY-NC)

where ρ captures the net effect of non-rainfall environmental factors such as temperature, nutrient availability, and salinity that influence bacterial proliferation. Rainfall is modeled explicitly through $\beta(\theta)$ to isolate its effect on transmission. Figure 1 illustrates a diagram for the dynamics of the transmission:

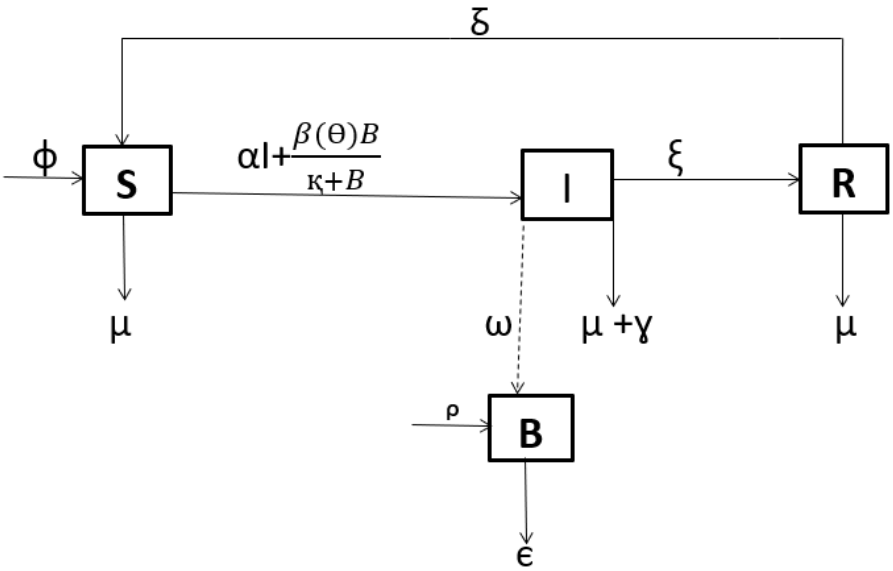

Figure 1: Flow diagram of rainfall-dependent cholera transmission model

The system of differential equations describing the model is:

$$\begin{aligned}
\frac{dS}{dt} &= \phi - \psi S - \mu S + \delta R \\
\frac{dI}{dt} &= \psi S - (\mu + \gamma) I - \xi I \\
\frac{dR}{dt} &= \xi I - \mu R - \delta R \\
\frac{dB}{dt} &= \rho B + \omega I - \epsilon B \\
Where; \psi &= \left[\alpha I + \frac{\beta(\theta) B}{\kappa + B} \right], \\
\beta(\theta) &= \beta_1 (1-\theta)^2 + \beta_2 \theta^2; \quad \beta_1 > \beta_2 \\
T &= \mu + \gamma + \xi.
\end{aligned} \tag{3}$$

Licensed Under Creative Commons Attribution (CC BY-NC)

2.2 Positivity and Boundedness

Since the model describes human and pathogen population, it should be well-posed. The positivity and boundedness of the solution of model (Figure 1) is determined using the following initial conditions:

$$\begin{cases} S(t_0) = S(0), \\ I(t_0) = I(0), \\ R(t_0) = R(0), \\ B(t_0) = B(0). \end{cases} \tag{4}$$

where $t_0 = 0$.

2.3 Positivity of the Solutions of the Model

Since the model describes the dynamics of a human population and pathogen concentration, all state variables must remain non-negative for all time $t \geq 0$, ensuring that the model's solution remains biologically meaningful.

Proposition 1. *Suppose that the initial conditions satisfy*

$$(S(0), I(0), R(0), B(0)) \in \mathbb{R}^4_+.$$

Then the solutions $S(t)$, $I(t)$, $R(t)$, and $B(t)$ of the cholera transmission model remain non-negative for all $t \geq 0$.

Proof. We show that each state variable remains non-negative for all $t \geq 0$ whenever the initial conditions are non-negative. Susceptible class:

From the model,

$$\frac{dS}{dt} = \phi - \psi S - \mu S + \delta R, \tag{5}$$

Since

$$\psi = \alpha I + \frac{\beta(\theta) B}{\kappa + B} \geq 0. \tag{6}$$

Therefore

$$\psi(\tau) = \alpha I(\tau) + \frac{\beta(\theta) B(\tau)}{\kappa + B(\tau)} \geq 0. \tag{7}$$

Thus,

$$\frac{dS}{dt} \geq -(\psi(t) + \mu) S. \tag{8}$$

Dividing both sides by $S(t) > 0$ and integrating from 0 to t gives:

$$\int_0^t \frac{1}{S(s)} \frac{dS}{ds} ds \geq -\int_0^t (\psi(s) + \mu)\, ds, \tag{9}$$

where s is a dummy variable of integration.

Evaluating the left-hand side and the right-hand side partially yield:

$$\ln S(t) - \ln S(0) \geq -\int_0^t (\psi(s) + \mu) ds\,. \tag{10}$$

Licensed Under Creative Commons Attribution (CC BY-NC)

Taking exponents on both sides, we obtain:

$$S(t) \geq S(0) \exp\left(- \int_0^t (\psi(s) + \mu) ds \right). \tag{11}$$

Since $\psi(s) \geq 0$ and $\mu > 0$, the exponential function is strictly positive. Since exponential function is strictly positive, it follows that,

$$S(t) \geq 0 \quad \text{for all } t \geq 0. \tag{12}$$

Similarly, when the same procedure is applied to the Infected, Recovered and Pathogen compartments, we obtain the following positive solutions respectively:

$$\begin{aligned} I(t) &\geq I(0)e^{-Tt} \geq 0, \quad \text{since} \quad \psi S \geq 0 \quad \forall t \geq 0 \\ R(t) &\geq R(0)e^{-(\mu+\delta)t} \geq 0, \quad \forall t \geq 0 \\ \frac{dB}{dt} &\geq -\epsilon B \implies B(t) \geq B(0)e^{-\epsilon t} \geq 0, \quad \forall t \geq 0 \end{aligned} \tag{13}$$

Hence, all the solution of model (3) given initial conditions (4) at any time t are positive. Therefore, both the human population and pathogen concentration remains non-negative. □

2.4 Boundedness of the Solutions of the Model

Since the model formulated describes human beings, the human population will always remain bounded.

Proposition 2. *The solutions of the cholera transmission model with non-negative initial conditions are uniformly bounded for all $t \geq 0$ in the feasible region*

$$\Omega = \left\{ (S, I, R, B) \in \mathbb{R}_+^4 : \ N \leq \frac{\phi}{\mu}, \ B \leq \frac{\omega\phi}{\mu(\epsilon - \rho)} \right\}.$$

Let $N(t) = S(t) + I(t) + R(t)$. From the system of equation (3), we have:

$$\frac{dN}{dt} = \phi - \mu(S + I + R) - \gamma I \tag{14}$$

Thus:

$$\frac{dN}{dt} = \phi - \mu N(t) - \gamma I \tag{15}$$

Since $I(t) \geq 0$, we have $-\gamma I \leq 0$. Therefore,

$$\frac{dN}{dt} \leq \phi - \mu N(t) \tag{16}$$

Multiplying (16) by the integrating factor, $e^{\mu t}$ yield;

$$\frac{d(Ne^{\mu t})}{dt} = \phi e^{\mu t} \tag{17}$$

Licensed Under Creative Commons Attribution (CC BY-NC)

Integrating both side yield;

$$N(t)e^{\mu t} = \frac{\phi e^{\mu t}}{\mu} + C \tag{18}$$

Dividing all sides by $IF = e^{\mu t}$ and by comparison theorem yield;

$$N(t) \leq \frac{\phi}{\mu} + Ce^{-\mu t} \tag{19}$$

But

$$C = N(0) - \frac{\phi}{\mu}$$

Taking limits as

$$t \to \infty$$

$$\lim_{t\to\infty} N(t) \leq \frac{\phi}{\mu} \tag{20}$$

$$N(t) \leq \frac{\phi}{\mu}, \quad \forall t \geq 0 \tag{21}$$

To show that the pathogen concentration $B(t)$ is bounded, consider the pathogen equation from system (3): Rearranging yield:

$$\frac{dB}{dt} = (\rho - \epsilon)B + \omega I. \tag{22}$$

From the boundedness of the total human population, we have:

$$N(t) = S(t) + I(t) + R(t) \leq \frac{\phi}{\mu}. \tag{23}$$

Since $I(t) \leq N(t)$, it follows that:

$$I(t) \leq \frac{\phi}{\mu}. \tag{24}$$

Hence,

$$\omega I(t) \leq \omega \frac{\phi}{\mu}. \tag{25}$$

Let

$$M = \omega \frac{\phi}{\mu}. \tag{26}$$

Then:

$$\frac{dB}{dt} \leq (\rho - \epsilon)B + M. \tag{27}$$

Since, $\epsilon > \rho$, we define $c = \epsilon - \rho > 0$.
Then equation (27) becomes:

$$\frac{dB}{dt} \leq -cB + M. \tag{28}$$

Consider the comparison equation:

$$\frac{dy}{dt} = -cy + M, \qquad y(0) = B(0). \tag{29}$$

Licensed Under Creative Commons Attribution (CC BY-NC)

Solving (29) using the integrating factor (e^{ct}) gives

$$\frac{d}{dt}(ye^{ct}) = Me^{ct}. \tag{30}$$

Integrating both sides gives

$$ye^{ct} = \frac{M}{c}e^{ct} + C. \tag{31}$$

Using the initial condition $y(0) = B(0)$ gives $C = B(0) - \frac{M}{c}$. Therefore:

$$y(t) = \frac{M}{c} + \left(B(0) - \frac{M}{c}\right)e^{-ct}. \tag{32}$$

By the comparison theorem (since $dB/dt \leq -cB + M$ and $dy/dt = -cy + M$ with the same initial condition), we have:

$$B(t) \leq y(t) = \frac{M}{c} + \left(B(0) - \frac{M}{c}\right)e^{-ct}. \tag{33}$$

Taking the limit as $t \to \infty$ we have:

$$\limsup_{t\to\infty} B(t) \leq \frac{M}{c}. \tag{34}$$

Substituting the value of M and c into (34), we obtain the uniform bound:

$$B(t) \leq \frac{\omega\phi}{\mu(\epsilon - \rho)} \quad \text{for all } t \geq 0, \tag{35}$$

provided that $\epsilon > \rho$ and $B(0)$ is finite.
Thus, the pathogen concentration remains bounded for all $t \geq 0$ under the condition $\epsilon > \rho$.
Since the solutions of the model are positive and bounded even in the presence of disease-induced deaths, then the model is well-posed.

2.5 The Basic Reproduction Number R_0

Definition 2.1. *The basic reproduction number R_0 is the average number of secondary infections produced by a single infectious individual introduced into a completely susceptible population.*
It serves as a threshold parameter that determines whether cholera can invade and persist within the population. It is computed using the next generation matrix approach as described in [6].

Proof. We consider the infected compartments I (infected humans) and B (pathogen concentration). Let $\mathcal{F}$ represent the rate of appearance of new infections, and $\mathcal{V}$ represent the transfer of individuals between compartments. The system for infected components is:

$$\begin{aligned} \frac{dI}{dt} &= \alpha IS + \frac{\beta(\theta)BS}{\kappa + B} - TI, \\ \frac{dB}{dt} &= \omega I + (\rho - \epsilon)B. \end{aligned} \tag{36}$$

Licensed Under Creative Commons Attribution (CC BY-NC)

At the Disease-Free Equilibrium (DFE):

$$E^0 = (S_0, 0, 0, 0), \quad \text{where } S_0 = \frac{\phi}{\mu}.$$

Linearizing the new infection terms of system (3) at the DFE yield;

$$\mathcal{F} = \begin{pmatrix} \alpha S_0 I + \frac{\beta(\theta) S_0}{\kappa + B} B \\ 0 \end{pmatrix} \tag{37}$$

The transition terms yield;

$$\mathcal{V} = \begin{pmatrix} (T)I \\ (\epsilon - \rho)B - \omega I \end{pmatrix} \tag{38}$$

The Jacobian matrices evaluated at the DFE are:

$$F = \begin{bmatrix} \alpha S_0 & \frac{\beta(\theta) S_0}{\kappa} \\ 0 & 0 \end{bmatrix}, \quad V = \begin{bmatrix} T & 0 \\ -\omega & \epsilon - \rho \end{bmatrix}, \tag{39}$$

The inverse of matrix V is:

$$V^{-1} = \begin{bmatrix} \frac{1}{T} & 0 \\ \frac{\omega}{(\epsilon-\rho)T} & \frac{1}{\epsilon-\rho} \end{bmatrix} \tag{40}$$

Thus,

$$FV^{-1} = \begin{bmatrix} \frac{\alpha S_0}{T} + \frac{\beta(\theta) S_0 \omega}{\kappa(\epsilon-\rho)(T)} & \frac{\beta(\theta) S_0}{\kappa(\epsilon-\rho)} \\ 0 & 0 \end{bmatrix} \tag{41}$$

The reproduction number is the spectral radius of the matrix FV^{-1};

$$R_0 = \frac{\alpha S_0}{T} + \frac{\beta(\theta) S_0 \omega}{\kappa(\epsilon - \rho)T} \tag{42}$$

Substituting $S_0 = \frac{\phi}{\mu}$ gives:

$$R_0 = \frac{\alpha \phi}{\mu T} + \frac{\beta(\theta)\, \phi\, \omega}{\mu \kappa T(\epsilon - \rho)}. \tag{43}$$

□

2.6 Disease Free Equilibrium Points (DFE)

Definition 2.2. *Disease Free Equilibrium Points (DFE) is the equilibrium state of an epidemiological model in which there no infection present in the human population.*

Proposition 3. *The cholera model (3.1) admits a biologically feasible disease-free equilibrium given by*

$$E^0 = \left(\frac{\phi}{\mu}, 0, 0, 0\right),$$

Licensed Under Creative Commons Attribution (CC BY-NC)

which represents the absence of cholera infection in both the human population and the environmental bacterial reservoir.
The disease-free equilibrium is obtained by setting the time derivatives of the state variables equal to zero;

$$\frac{dS}{dt} = \frac{dI}{dt} = \frac{dR}{dt} = \frac{dB}{dt} = 0,$$

and assuming; $I = 0$, $R = 0$, $B = 0$.

Proof. Substituting these conditions into the system of equations (3) gives

$$\frac{dS}{dt} = \phi - \mu S \tag{44}$$

Setting (44) to zero and making S the subject of the formula yield:

$$S = \frac{\phi}{\mu} \tag{45}$$

Hence, DFE: $E^0(S^0, I^0, R^0, B^0) = E^0(\frac{\phi}{\mu}, 0, 0, 0)$.
Therefore, the model possesses a biologically feasible disease-free equilibrium, representing the absence of cholera infection in both the human population and the environment.

2.7 Endemic Equilibrium Points (EE)

Definition 2.3. *Is the steady state of the model at which the infection persists in the population at a constant level over time. In this model, this means that the infected individuals and the bacteria Vibrio cholerae remain present in the human and environmental populations, respectively, while the all compartments remains constant over time.*

Theorem 2.1. *The cholera model (3) admits a endemic equilibrium given by*

$$E^* = (S^*, I^*, R^*, B^*)$$

whenever $R_0 > 1$.

The endemic equilibrium of the model is obtained by setting the equations to zero such that

$$\begin{aligned} \frac{dS}{dt} = \phi - \psi S^* - \mu S^* + \delta R^* &= 0 \\ \frac{dI}{dt} = \psi S^* - (T) I^* &= 0 \\ \frac{dR}{dt} = \xi I^* - (\mu + \delta) R^* &= 0 \\ \frac{dB}{dt} = (\rho - \epsilon) B^* + \omega I^* &= 0 \end{aligned} \tag{46}$$

Evaluating $\frac{dR}{dt} = \frac{dB}{dt} = 0$, we obtain the endemic equilibrium of pathogen population and recovered individuals as

$$R^* = \frac{\xi I^*}{\mu + \delta}, \quad B^* = \frac{\omega I^*}{\epsilon - \rho} \tag{47}$$

Licensed Under Creative Commons Attribution (CC BY-NC)

Recall that

$$\psi = \alpha I^* + \frac{\beta(\theta)B^*}{\kappa + B^*},$$

Substituting ψ into $\frac{dI}{dt} = 0$ then dividing by I all through gives

$$S^* = \frac{T\left[\kappa(\epsilon - \rho) + \omega I^*\right]}{\alpha\left[\kappa(\epsilon - \rho) + \omega I^*\right] + \beta(\theta)\omega} \tag{48}$$

Substituting R^* into $\frac{dS}{dt} = 0$ gives

$$\phi = TI^* + \mu S^* - \delta\left(\frac{\xi I^*}{\mu + \delta}\right). \tag{49}$$

Rearrange the formula we obtain

$$I^* = \frac{\phi - \mu S^*}{\left[T - \frac{\delta\xi}{\mu+\delta}\right]} \tag{50}$$

Thus, the endemic equilibrium is

$$E^*(S^*, I^*, R^*, B^*) = \left(\frac{T\left[\kappa(\epsilon - \rho) + \omega I^*\right]}{\alpha\left[\kappa(\epsilon - \rho) + \omega I^*\right] + \beta(\theta)\omega}, \frac{\phi - \mu S^*}{\left[T - \frac{\delta\xi}{\mu+\delta}\right]}, \frac{\xi I^*}{\mu + \delta}, \frac{\omega I^*}{\epsilon - \rho}\right)$$

Therefore, the model possesses a biologically feasible endemic equilibrium whenever $R_0 > 1$. □

2.8 Local Stability of the Disease Free Equilibrium Point (DFE)

The disease-free equilibrium is said to be locally asymptotically stable if solutions of the cholera transmission model that start sufficiently close to the DFE remain close to it and converge to the DFE as$t \to \infty$.

For the cholera model, the DFE is locally asymptotically stable when all eigenvalues of the Jacobian matrix evaluated at the DFE have negative real parts, meaning that a small introduction of cholera into a disease-free population will eventually die out.

Proposition 4. *The disease-free equilibrium*

$$E_0 = \left(\frac{\phi}{\mu}, 0, 0, 0\right)$$

is locally asymptotically stable if $R_0 < 1$ *and unstable if* $R_0 > 1$.

Proof. The Jacobian matrix of the system (3) is given by:

$$J = \begin{bmatrix} -\psi - \mu & -\alpha S & \delta & \frac{-\beta(\theta)\kappa S}{(\kappa+B)^2} \\ \psi & \alpha S - T & 0 & \frac{\beta(\theta)\kappa S}{(\kappa+B)^2} \\ 0 & \xi & -(\mu + \delta) & 0 \\ 0 & \omega & 0 & \rho - \epsilon \end{bmatrix} \tag{51}$$

Licensed Under Creative Commons Attribution (CC BY-NC)

Evaluating the jacobian matrix at the disease-free equilibrium $E_0 = (\frac{\phi}{\mu}, 0, 0, 0)$ gives

$$J(E_0) = \begin{bmatrix} -\mu & -\alpha\frac{\phi}{\mu} & \delta & \frac{-\beta(\theta)\phi}{\mu\kappa} \\ 0 & \alpha\frac{\phi}{\mu} - T & 0 & \frac{\beta(\theta)\phi}{\mu\kappa} \\ 0 & \xi & -(\mu+\delta) & 0 \\ 0 & \omega & 0 & \rho - \epsilon \end{bmatrix} \tag{52}$$

The characteristic equation of the infected and uninfected subsystems are obtained from

$$|J_{11} - \lambda I| = \left| \begin{pmatrix} -\mu - \lambda & \delta \\ 0 & -(\mu+\delta) - \lambda \end{pmatrix} \right| = 0.$$

and

$$|J_{22} - \lambda I| = \left| \begin{pmatrix} \alpha\frac{\phi}{\mu} - T - \lambda & \frac{\beta(\theta)\phi}{\mu\kappa} \\ \omega & \rho - \epsilon - \lambda \end{pmatrix} \right| = 0.$$

The eigenvalues of $J(E_0)$ consist of the eigenvalues of J_{11} and J_{22}. Therefore characteristic equation associated with determinant of J_{11} is

$$\lambda^2 + (2\mu + \delta)\lambda + \mu(\mu + \delta) = 0. \tag{53}$$

Solving the equation (53) yields the eigenvalues of the uninfected subsystem matrix as

$$\lambda_1 = -\mu, \qquad \lambda_2 = -(\mu + \delta), \tag{54}$$

which are both negative.
The characteristic equation associated with determinant of J_{22} is

$$\lambda^2 - \left(\frac{\alpha\phi}{\mu} - T - (\epsilon - \rho)\right)\lambda + \left(T - \frac{\alpha\phi}{\mu}\right)(\epsilon - \rho) - \frac{\beta(\theta)\phi\omega}{\mu\kappa} = 0. \tag{55}$$

By the Routh–Hurwitz criterion[20], the eigenvalues of the infected subsystem matrix J_{22} have negative real parts if

$$\text{tr}(J_{22}) < 0 \qquad \text{and} \qquad \det(J_{22}) > 0.$$

Let M and N denote the trace and the determinant of the infected subsystem respectively, where,

$$M = \frac{\alpha\phi}{\mu} - T - (\epsilon - \rho) \tag{56}$$

and

$$N = \left(T - \frac{\alpha\phi}{\mu}\right)(\epsilon - \rho) - \frac{\beta(\theta)\phi\omega}{\mu\kappa}. \tag{57}$$

Then, the characteristic equation can be expressed as

$$\lambda^2 - M\lambda + N = 0. \tag{58}$$

Licensed Under Creative Commons Attribution (CC BY-NC)

Recall that the basic reproduction number is given by

$$R_0 = \frac{\alpha\phi}{\mu T} + \frac{\beta(\theta)\phi\omega}{\mu\kappa T(\epsilon - \rho)}. \tag{59}$$

Multiplying both sides by $T(\epsilon - \rho)$ gives

$$T(\epsilon - \rho)R_0 = \frac{\alpha\phi}{\mu}(\epsilon - \rho) + \frac{\beta(\theta)\phi\omega}{\mu\kappa}. \tag{60}$$

Hence,

$$\begin{aligned} T(\epsilon - \rho)(1 - R_0) &= T(\epsilon - \rho) - T(\epsilon - \rho)R_0 \\ &= T(\epsilon - \rho) - \left[\frac{\alpha\phi}{\mu}(\epsilon - \rho) + \frac{\beta(\theta)\phi\omega}{\mu\kappa}\right] \\ &= \left(T - \frac{\alpha\phi}{\mu}\right)(\epsilon - \rho) - \frac{\beta(\theta)\phi\omega}{\mu\kappa}. \end{aligned} \tag{61}$$

Since

$$N = \left(T - \frac{\alpha\phi}{\mu}\right)(\epsilon - \rho) - \frac{\beta(\theta)\phi\omega}{\mu\kappa},$$

it follows that

$$N = T(\epsilon - \rho)(1 - R_0). \tag{62}$$

Therefore, whenever $R_0 < 1$, and $\epsilon > \rho$, we have

$$N > 0.$$

Conversely, since $\frac{\alpha\phi}{\mu} < T$,and $\epsilon > \rho$, it follows that

$$M < 0.$$

Thus, the Routh–Hurwitz conditions are satisfied whenever $R_0 < 1$ and $\epsilon > \rho$. Consequently, the infected subsystem is locally asymptotically stable. Since the eigenvalues of the uninfected subsystem are also negative, all eigenvalues of the Jacobian matrix evaluated at E_0 have negative real parts. Therefore, the disease-free equilibrium E_0 is locally asymptotically stable. □

2.9 Global Stability of the Disease Free Equilibrium Point (DFE)

The disease-free equilibrium is said to be globally asymptotically stable if every solution of the cholera transmission model that starts in the biologically feasible region converges to the DFE as $t \to \infty$. Thus, regardless of the initial population sizes, the system eventually approaches the disease-free state.

Proposition 5. *The DFE of the system (3) is globally asymptotically stable if* $R_0 < 1$.

To study the Global asymptotic stability of the DFE, we use the method introduced by Castillo-Chavez.

Licensed Under Creative Commons Attribution (CC BY-NC)

Lemma 1 (Castillo-Chavez[3]). *Consider a model system written in the form:*

$$\frac{dX_1}{dt} = F(X_1, X_2)$$

$$\frac{dX_2}{dt} = G(X_1, X_2), \quad G(X_1, 0) = 0$$

where $X_1 \in \mathbb{R}^n$ *represents the vector of uninfected components* (S, R) *while* $X_2 \in \mathbb{R}^n$ *represents the vector of infected components* (I, B).
Let $X_0 = (X_1^*, 0)$ denotes the (DFE) of the system.
Also assume the conditions (H_1) and (H_2) below:
(H_1) For $\frac{dX_1}{dt} = F(X_1, 0)$, X_1^* is globally asymptotically stable.
(H_2) $G(X_1, X_2) = AX_2 - \hat{G}(X_1, X_2)$, $\hat{G}(X_1, X_2) \geq 0$ for $(X_1, X_2) \in \Omega$,
where the Jacobian $A = \left(\frac{\partial G}{\partial X_2}\right)(X_1^*, 0)$ is an M-matrix (the off-diagonal elements of A are non-negative) and Ω is the biologically feasible region.
Then the DFE $X_0 = (X_1^*, 0)$ is globally asymptotically stable provided that $R_0 < 1$.

Proof. We adopt the notations in the Lemma and verify conditions (H_1) and (H_2). In our model, $X_1 = (S, R)^T$, $X_2 = (I, B)^T$ and $X_1^* = (\frac{\phi}{\mu}, 0)^T$.
The uninfected sub-system is:

$$\frac{d}{dt}\begin{pmatrix} S \\ R \end{pmatrix} = F(X_1, 0) = \begin{bmatrix} \phi - \mu S + \delta R \\ \xi I - (\mu + \delta)R \end{bmatrix} \tag{63}$$

and the infected system is:

$$\frac{d}{dt}\begin{pmatrix} I \\ B \end{pmatrix} = G = \begin{bmatrix} \psi S - (T)I \\ (\rho - \epsilon)B + \omega I \end{bmatrix} \tag{64}$$

To obtain the solutions for S and R, we take the integral of (63) as follows; From equation two of (63), we have

$$\int_0^t \frac{dR}{R} = -(\mu + \delta)\int dt \tag{65}$$

$$\ln(R) = -(\mu + \delta)t + C \tag{66}$$

$$R(t) = R(0)e^{-(\mu+\delta)t} \tag{67}$$

As $t \to \infty$ then, $R(t) \to 0$. Similarly, from the first equation of (63), since $R(t) \to 0$ as $t \to \infty$ we have:

$$\int_0^t \frac{dS}{\phi - \mu S} = \int dt \tag{68}$$

$$-\mu \ln\left(\frac{\phi - \mu S(t)}{\phi - \mu S(0)}\right) = t + C \tag{69}$$

$$\frac{\phi - \mu S(t)}{\phi - \mu S(0)} = e^{-\mu t} \quad \text{where } C \text{ is a constant} \tag{70}$$

Licensed Under Creative Commons Attribution (CC BY-NC)

$$S(t) = \frac{\phi}{\mu} - \left(\frac{\phi - \mu S(0)}{\mu}\right) e^{-\mu t} \tag{71}$$

As $t \to \infty$ at DFE, then:

$$S(t) = \frac{\phi}{\mu} \tag{72}$$

Clearly, $R(t) \to 0$ and $S(t) \to N = \frac{\phi}{\mu}$ as $t \to \infty$ regardless of the values of $R(0)$ and $S(0)$.
Hence, $X_1^* = (\frac{\phi}{\mu}, 0)$ is globally asymptotically stable for the sub-system $\frac{dX_1}{dt} = F(X_1, 0)$.
To verify condition (H_2) of the Castillo–Chavez lemma, we write

$$G(X_1, X_2) = AX_2 - \hat{G}(X_1, X_2),$$

where A is the Jacobian matrix of the infected subsystem with respect to the infected variables (I, B), evaluated at the disease-free equilibrium.

$$A = \begin{bmatrix} \alpha S^* - T & \frac{\beta(\theta) S^*}{\kappa} \\ \omega & \rho - \epsilon \end{bmatrix}. \tag{73}$$

The off-diagonal entries of A are

$$\frac{\beta(\theta) S^*}{\kappa} \quad \text{and} \quad \omega, \tag{74}$$

which are non-negative since $\beta(\theta) > 0$, $S^* > 0$, $\kappa > 0$, and $\omega > 0$. Hence, A is an M-matrix.
Therefore,

$$AX_2 = \begin{bmatrix} (\alpha S^* - T) I + \frac{\beta(\theta) S^*}{\kappa} B \\ \omega I + (\rho - \epsilon) B \end{bmatrix}. \tag{75}$$

Consequently, the nonlinear part is given by

$$\hat{G}(X_1, X_2) = AX_2 - G(X_1, X_2),$$

which gives

$$\hat{G}(X_1, X_2) = \begin{pmatrix} \alpha(S^* - S) I + \frac{\beta(\theta) S^*}{\kappa} B - \frac{\beta(\theta) S B}{\kappa + B} \\ 0 \end{pmatrix}. \tag{76}$$

Since the feasible region satisfies $N(t) \leq \frac{\phi}{\mu} = S^*$, and $S(t) \leq N(t)$,it follows that $S(t) \leq S^*$,so that $\alpha(S^* - S) I \geq 0$.
Moreover, since $\kappa + B \geq \kappa$,we have

$$\frac{S^*}{\kappa} \geq \frac{S}{\kappa + B},$$

and therefore

$$\frac{\beta(\theta) S^*}{\kappa} B - \frac{\beta(\theta) S B}{\kappa + B} \geq 0.$$

Licensed Under Creative Commons Attribution (CC BY-NC)

Hence,

$$\hat{G}(X_1, X_2) \geq 0$$

for all $(X_1, X_2) \in \Omega$. Hence, condition (H_2) is satisfied.
Since, conditions (H_1) and (H_2) of the Castillo–Chavez lemma are satisfied, it follows that disease-free equilibrium

$$E^0 = \left(\frac{\phi}{\mu}, 0, 0, 0\right)$$

is globally asymptotically stable whenever $R_0 < 1$. □

2.10 Local Stability of the Endemic Equilibrium (EE)

The endemic equilibrium is said to be locally asymptotically stable if solutions of the cholera transmission model that start sufficiently close to the endemic equilibrium remain close to it and converge to the endemic equilibrium as$t \to \infty$.
In this study, the local stability of the endemic equilibrium is determined by evaluating the Jacobian matrix of the model at E^*. The endemic equilibrium is locally asymptotically stable if all eigenvalues of the Jacobian matrix evaluated at E^* have negative real parts.
Proposition 6. *Suppose that the endemic equilibrium*

$$E^* = (S^*, I^*, R^*, B^*)$$

exists. If the coefficients of the characteristic polynomial of the Jacobian matrix evaluated at E^* satisfy the Routh–Hurwitz conditions, then the endemic equilibrium E^* is locally asymptotically stable.

Proof. The Jacobian matrix of the system evaluated at the endemic equilibrium E^* is

$$J(E^*) = \begin{bmatrix} -\psi^* - \mu & -\alpha S^* & \delta & -C \\ \psi^* & \alpha S^* - T & 0 & C \\ 0 & \xi & -(\mu + \delta) & 0 \\ 0 & \omega & 0 & \rho - \epsilon \end{bmatrix}, \tag{77}$$

where

$$C = \frac{\beta(\theta)\kappa S^*}{(\kappa + B^*)^2}.$$

The characteristic polynomial associated with the jacobian matrix is obtained from

$$J(E^*) - \lambda I = \begin{bmatrix} -\psi^* - \mu - \lambda & -\alpha S^* & \delta & -C \\ \psi^* & \alpha S^* - T - \lambda & 0 & C \\ 0 & \xi & -(\mu + \delta) - \lambda & 0 \\ 0 & \omega & 0 & (\rho - \epsilon) - \lambda \end{bmatrix}. \tag{78}$$

and it can be expressed as

$$\lambda^4 + a_1\lambda^3 + a_2\lambda^2 + a_3\lambda + a_4 = 0,$$

where $a_1, \quad a_2, \quad a_3 \quad and \quad a_4$ are coefficients.

Licensed Under Creative Commons Attribution (CC BY-NC)

Applying the Routh-Hurwitz criterion [20], the characteristic polynomial has all its roots with negative real parts if $a_1 > 0, \quad a_2 > 0, \quad a_3 > 0, \quad a_4 > 0 \quad , a_1 a_2 > a_3 \quad and \quad a_1 a_2 a_3 > a_3^2 + a_1^2 a_4$ are satisfied. The coefficients of the characteristic polynomial are given by

$$\begin{aligned}
a_1 &= (\psi^* + \mu) + (T - \alpha S^*) + (\mu + \delta) + (\epsilon - \rho), \\
a_2 &= (\psi^* + \mu)(T - \alpha S^*) + (\psi^* + \mu)(\mu + \delta) \\
&\quad + (\psi^* + \mu)(\epsilon - \rho) + (T - \alpha S^*)(\mu + \delta) \\
&\quad + (T - \alpha S^*)(\epsilon - \rho) + (\mu + \delta)(\epsilon - \rho) + \alpha S^* \psi^* - C\omega, \\
a_3 &= (\psi^* + \mu)(T - \alpha S^*)(\mu + \delta) + (\psi^* + \mu)(T - \alpha S^*)(\epsilon - \rho) \\
&\quad + (\psi^* + \mu)(\mu + \delta)(\epsilon - \rho) + (T - \alpha S^*)(\mu + \delta)(\epsilon - \rho) \\
&\quad + \alpha S^* \psi^* (\mu + \delta) + \alpha S^* \psi^* (\epsilon - \rho) - \delta \xi \psi^* - C\omega(2\mu + \delta), \\
a_4 &= (\psi^* + \mu)(T - \alpha S^*)(\mu + \delta)(\epsilon - \rho) + \alpha S^* \psi^* (\mu + \delta)(\epsilon - \rho) \\
&\quad - \delta \xi \psi^* (\epsilon - \rho) - C\omega\mu(\mu + \delta).
\end{aligned} \tag{79}$$

Defining the two remaining Routh-Hurwitz conditions by

$$H_1 = a_1 a_2 - a_3 \quad and \quad H_2 = a_1 a_2 a_3 - a_3^2 - a_1^2 a_4, \tag{80}$$

gives

$$H_1 > 0, \qquad H_2 > 0. \tag{81}$$

Therefore, provided that $a_i > 0$ where, $i = 1, 2, 3, 4$ and $H_1 > 0, \quad H_2 > 0$, the Routh-Hurwitz criterion is satisfied. Consequently, all eigenvalues of $J(E^*)$ have negative real parts, and the endemic equilibrium E^* is locally asymptotically stable. □

3 Numerical Simulations and Results

Using the parameter values derived from published epidemiological studies, WHO reports and literature on cholera outbreaks in table 1 and the initial conditions in table 2 below, numerical simulation results were obtained. The initial conditions for the numerical simulation were assumed to represent a typical ongoing cholera outbreak scenario in a representative urban community such Nairobi, where high population density, frequent human interactions and dependence on shared water and sanitation infrastructure facilitate the spread of cholera. According to the 2019 Kenya Population and Housing Census, Nairobi county had an approximate population of 4,397,073 people[9].

Licensed Under Creative Commons Attribution (CC BY-NC)

Table 1: Parameter Values Used for Quantitative Sensitivity Analysis

Parameter	**Symbol**	**Value**	**Ref.**
Recruitment rate	ϕ	1000 persons/day	[25]
Natural death rate	μ	0.00027 day^{-1}	[26]
Human-to-human transmission rate	α	5.0×10^{-8} $\text{person}^{-1}\text{day}^{-1}$	Estimated
Environmental transmission rate (baseline)	$\beta(\theta)$	0.01 day^{-1}	[13]
Environment-to-human transmission (heavy rainfall)	β_1	0.03 day^{-1}	Estimated
Environment-to-human transmission (drought)	β_2	0.025 day^{-1}	Estimated
Rainfall parameter	θ	[0,1]	Estimated
Half-saturation constant	κ	10^6 cells/ml	[8, 5]
Recovery rate	ξ	0.2 day^{-1}	[24]
Loss of immunity rate	δ	0.003 day^{-1}	Estimated
Disease-induced death rate	γ	0.0002 day^{-1}	[26]
Pathogen shedding rate	ω	1 cell/ml/person/day	[14]
Pathogen growth rate	ρ	0.35 day^{-1}	[5]
Pathogen death rate	ϵ	0.68 day^{-1}	[5, 8]

The value for the pathogen shedding rate was selected based on literature range and numerical exploration to produce realistic environmental bacterial dynamics, while avoiding excessive accumulation of bacteria in the environmental reservoir. A relatively small human-to-human transmission rate was adopted on the assumption that environmental transmission is the dominant transmission pathway in the present model and examined through sensitivity analysis. The rainfall-dependent environmental transmission rates were selected through numerical exploration using a literature-informed baseline for environmental transmission to represent the two rainfall extremes. The loss of immunity rate was assumed based on an approximately one-year duration of temporal immunity.

Table 2: Initial Conditions for Numerical Simulation

Compartment	**Variable**	**Initial Value**	**Ref.**
Susceptible individuals	$S(0)$	3,703,704 persons	[25, 26]
Infected individuals	$I(0)$	30000 persons	Estimated
Recovered individuals	$R(0)$	30000 persons	Estimated
Pathogen concentration	$B(0)$	100,000 cells/ml	Estimated

The SIR curves generated by the cholera model reveal classic epidemic patterns that provide crucial insights into disease dynamics.

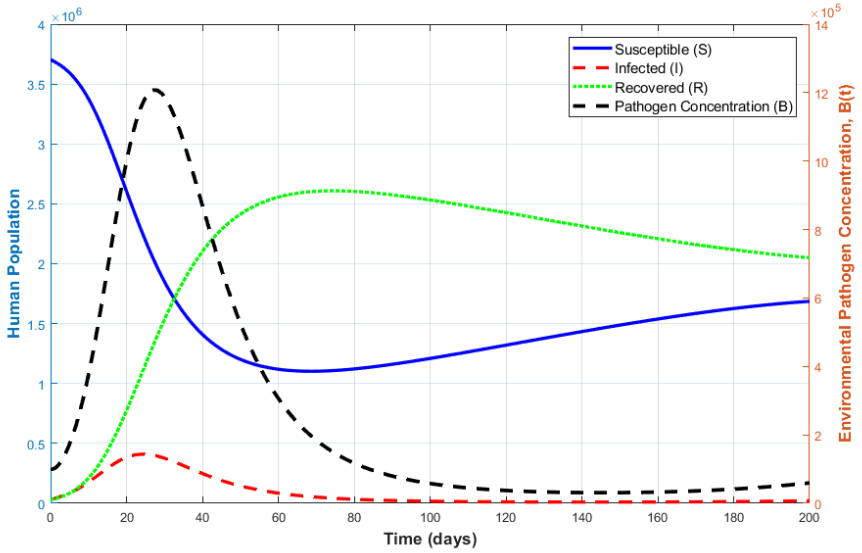

Figure 2: Combined SIR-B dynamics over time

Figure 2 illustrates the interaction between the human population and the environmental reservoir of *Vibrio cholerae* over time, highlighting how rainfall variation influences cholera transmission through changes in environmental contamination.

The numerical simulations demonstrate that rainfall variation plays a significant role in shaping cholera disease dynamics by influencing the environmental transmission pathway. The combined SIR-B dynamics show a strong interaction between the human population and the environmental reservoir of *Vibrio cholerae*, confirming that disease transmission is sustained through both direct human-to-human contact and environmental contamination. However, the simulations consistently indicate that the environmental pathway contributes more substantially to the overall transmission potential than direct human-to-human transmission.

Licensed Under Creative Commons Attribution (CC BY-NC)

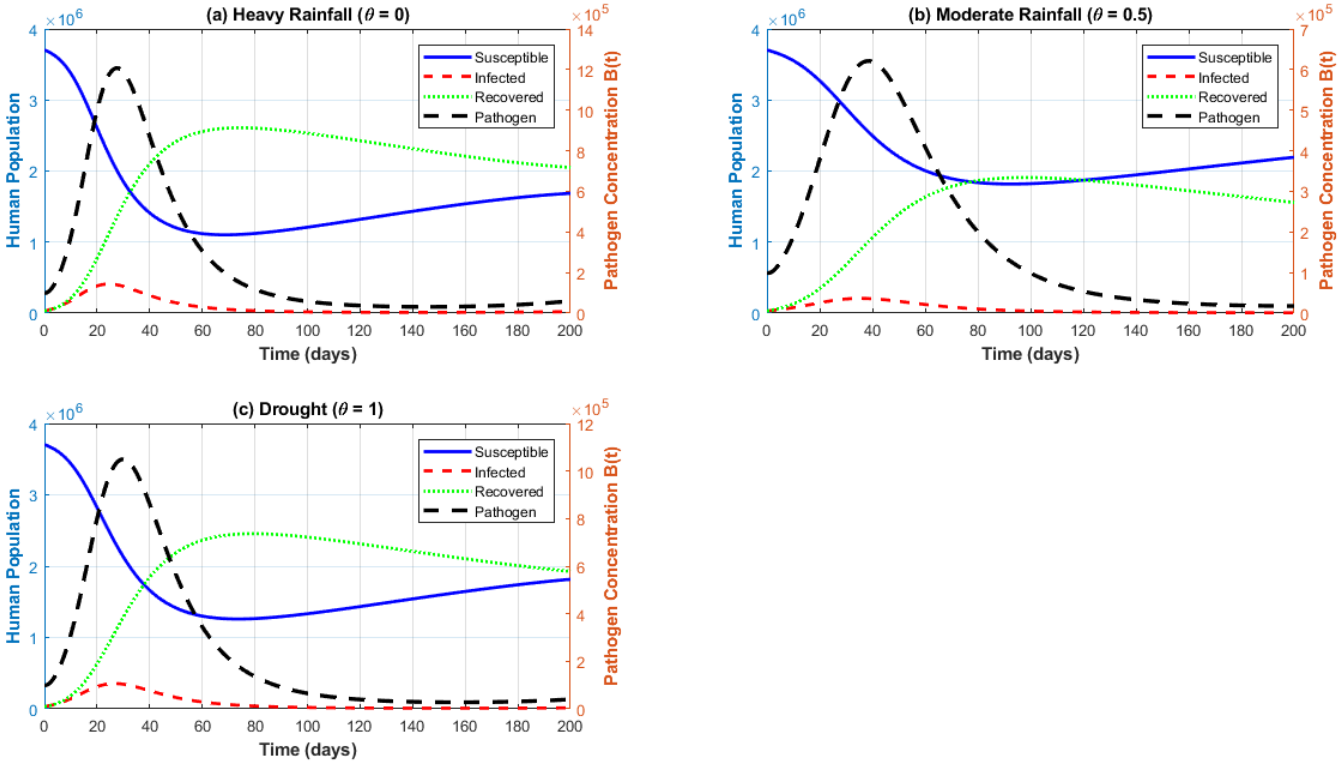

Figure 3: Effect of rainfall variation on cholera transmission dynamics under three rainfall scenarios

Figure 3(a) describes disease dynamics under heavy rainfall conditions ($\theta = 0$).
Figure 3(b) demonstrates disease dynamics under moderate rainfall conditions ($\theta = 0.5$).
Figure 3(c)Demonstrates the disease dynamics under drought conditions ($\theta = 1$).
Comparison of the three rainfall conditions revealed distinct transmission patterns. Heavy rainfall produced the highest disease burden, characterized by the fastest decline in the susceptible population, the highest peak in infected individuals, and the greatest accumulation of environmental pathogens. This behavior reflects the ability of flooding to disperse *Vibrio cholerae* into water sources, thereby increasing exposure to contaminated water and enhancing environmental transmission. In contrast, moderate rainfall generated the lowest infection levels and the smallest environmental pathogen concentration, suggesting that favorable water and sanitation conditions reduce environmental contamination and limit disease transmission. Drought exhibited an intermediate pattern, where limited water availability increased reliance on contaminated water sources, leading to higher transmission than under moderate rainfall but lower transmission than under heavy rainfall.

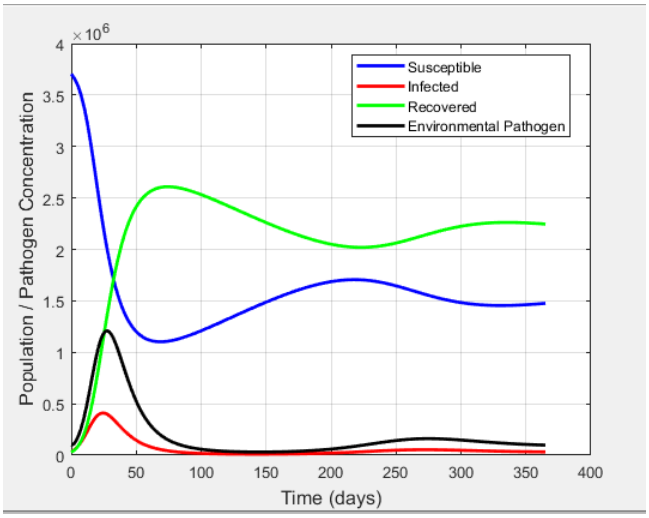

Figure 4: Endemic equilibrium ($R_0 > 1$)

Figure in 4 initially shows that susceptible population is high, while the infected and recovered populations represent only a small proportion of the total population. The environmental concentration of *Vibrio cholerae* is also initially positive due to contamination from infected individuals. The simulated trajectories further showed that all model compartments converged to positive equilibrium values, indicating the persistence of cholera within the population. Consequently, the disease-free equilibrium remained unstable, while the endemic equilibrium was locally asymptotically stable. Although moderate rainfall reduced the transmission potential, the corresponding reproduction number remained greater than one, indicating that cholera could still persist unless additional intervention measures were implemented.

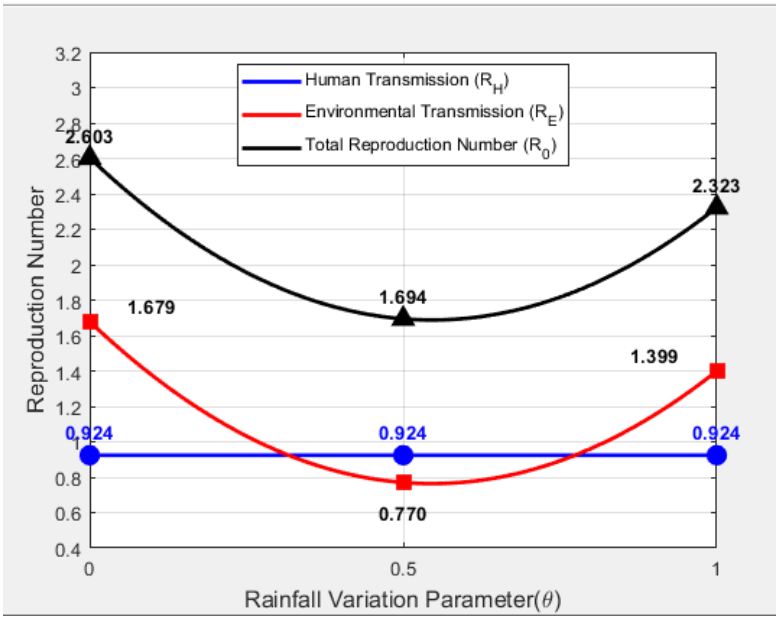

Figure 5: Reproduction numbers for different rainfall conditions

Licensed Under Creative Commons Attribution (CC BY-NC)

The graphs show the stability of the endemic equilibrium (EE), which is established when ($R_0 > 1$), and the disease-free equilibrium (DFE), which is established when ($R_0 < 1$).
Analysis of the reproduction numbers demonstrated that rainfall variation substantially influences the environmental component of transmission. The environmental reproduction number was highest under heavy rainfall, lowest under moderate rainfall, and increased again under drought conditions, producing a U-shaped relationship between rainfall and transmission potential. Since the environmental reproduction number constituted a large proportion of the total basic reproduction number across all rainfall conditions, the simulations confirm that environmental transmission is the dominant pathway in the proposed model.

4 Conclusion and Recommendations

4.1 Conclusion

This study developed and analyzed a rainfall-dependent SIR-B cholera model to investigate the effect of rainfall variation on cholera transmission dynamics. The model incorporates both direct human-to-human transmission and indirect environmental transmission through the reservoir of *Vibrio cholerae*, with rainfall variation incorporated through a nonlinear environmental transmission coefficient. Analytical results established the positivity and boundedness of solutions, while the disease-free and endemic equilibria were derived and their stability investigated using the basic reproduction number.

4.2 Recommendations

Based on the findings of this study, it is recommended that public health authorities should prioritize interventions that reduce environmental contamination by improving access to safe drinking water, strengthening sanitation infrastructure, and promoting hygiene practices, particularly during periods of heavy rainfall and drought when the risk of cholera transmission is highest. Also, cholera surveillance systems should incorporate rainfall and climate information into early warning systems to facilitate timely implementation of preventive and control measures before outbreaks escalate into epidemics. Since environmental transmission was found to contribute substantially to the overall basic reproduction number, cholera control programmes should integrate environmental management strategies, including protection of water sources, effective drainage systems, and rapid response to flooding events.

Declaration of Interest

The author declares that he doesn't have any known competing financial interests or personal relationships that could have appeared to influence the work reported in this paper.

Funding Declaration

This research did not receive any specific grant from funding agencies in the public, commercial, or not-for-profit sectors.

Licensed Under Creative Commons Attribution (CC BY-NC)

References

[1] Akinpelu, F., & Ojo, M. (2016). A mathematical model for the dynamic spread of infection caused by poverty and prostitution in Nigeria. *International Journal of Mathematical and Physical Sciences Research*, 4, 33–47

[2] Asadgol, Z., Mohammadi, H., Kermani, M., Badirzadeh, A., & Gholami, M. (2019). The effect of climate change on cholera disease: The road ahead using artificial neural network. *PLOS ONE*, 14(11), e0224813. https://doi.org/10.1371/journal.pone.0224813

[3] Castillo-Chavez, C., Feng, Z., & Huang, W. (2002). On the computation of R_0 and its role on global stability. In C. Castillo-Chavez et al. (Eds.), *Mathematical Approaches for Emerging and Reemerging Infectious Diseases* (pp. 229–250). Springer. https://doi.org/10.1007/978-1-4615-1045-9_13

[4] Charnley, G. E., Kelman, I., Green, N., Hinsley, W., Gaythorpe, K. A., & Murray, K. A. (2021). Exploring relationships between drought and epidemic cholera in Africa using generalised linear models. *BMC Infectious Diseases*, 21, 1–12. https://doi.org/10.1186/s12879-021-06662-4

[5] Codeço, C. T. (2001). Endemic and epidemic dynamics of cholera: The role of the aquatic reservoir. *BMC Infectious Diseases*, 1, 1–14. https://doi.org/10.1186/1471-2334-1-1

[6] Diekmann, O., Heesterbeek, J. A. P., & Roberts, M. G. (2010). The construction of next-generation matrices for compartmental epidemic models. *Journal of the Royal Society Interface*, 7(47), 873–885. https://doi.org/10.1098/rsif.2009.0386

[7] Hashizume, M., Armstrong, B., Hajat, S., Wagatsuma, Y., Faruque, A. S., Hayashi, T., & Sack, D. A. (2008). The effect of rainfall on the incidence of cholera in Bangladesh. *Epidemiology*, 19(1), 103–110. https://doi.org/10.1097/EDE.0b013e31815c09ea

[8] Jensen, M. A., Faruque, S. M., Mekalanos, J. J., & Levin, B. R. (2016). Modeling the role of bacteriophage in the control of cholera outbreaks. *Proceedings of the National Academy of Sciences*, 113(48), 13696–13701. https://doi.org/10.1073/pnas.1610101113

[9] Kenya National Bureau of Statistics. (2023).*2019 Kenya Population and Housing Census: Urban Population, Households and Density by County.* https://www.knbs.or.ke/wp-content/uploads/2023/09/2019-Kenya-population-and-Housing-Census-Urban-population-households-density- by-county.xlsx

[10] Koelle, K. (2009). The impact of climate on the disease dynamics of cholera. *Clinical Microbiology and Infection*, 15, 29–31. https://doi.org/10.1111/j.1469-0691.2009.02832.x

[11] Longini, I. M., Nizam, A., Ali, M., Yunus, M., Shenvi, N., & Clemens, J. D. (2007). Controlling endemic cholera with oral vaccines. *PLoS Medicine*, 4(11), e336. https://doi.org/10.1371/journal.pmed.0040336

[12] Moore, S. M., Azman, A. S., Zaitchik, B. F., Mintz, E. D., Brunkard, J., Legros, D., & Lessler, J. (2017). El Niño and the shifting geography of cholera in Africa. *Proceedings of the National Academy of Sciences*, 114(17), 4436–4441. https://doi.org/10.1073/pnas.1619218114

[13] Mukandavire, Z., Liao, S., Wang, J., Gaff, H., Smith, D. L., & Morris, J. G. (2011). Estimating the reproductive numbers for the 2008–2009 cholera outbreaks in Zimbabwe. *Proceedings of the National Academy of Sciences*, 108(21), 8767–8772. https://doi.org/10.1073/pnas.1019712108

[14] Nelson, E. J., Harris, J. B., Morris, J. G., Calderwood, S. B., & Camilli, A. (2009). Cholera transmission: The host, pathogen and bacteriophage dynamic. *Nature Reviews Microbiology*, 7(10), 693–702. https://doi.org/10.1038/nrmicro2204

[15] Nichols, G., Lake, I., & Heaviside, C. (2018). Climate change and water-related infectious diseases. *Atmosphere*, 9(10), 385. https://doi.org/10.3390/atmos9100385

[16] Owade, K. J., Akinyi, C., & Owour, G. L. (2018). Modeling the role of re-hydration and antibiotic

treatment on reduction of cholera mortality. *LOSR Journal of Mathematics*, 14(1), 11–21.

[17] Pollak, H. O. (2011). What is mathematical modeling? *Journal of Mathematics Education at Teachers College*, 2(1).

[18] Rieckmann, A., Tamason, C. C., Gurley, E. S., Rod, N. H., & Jensen, P. K. M. (2018). Exploring droughts and floods and their association with cholera outbreaks in sub-Saharan Africa: A register-based ecological study from 1990 to 2010. *The American Journal of Tropical Medicine and Hygiene*, 98(5), 1269–1275. https://doi.org/10.4269/ajtmh.17-0789

[19] Reyburn, R., Deen, J. L., Grais, R. F., Bhattacharya, S. K., Sur, D., Lopez, A. L., Jiddawi, M. S., Clemens, J. D., & von Seidlein, L. (2011). The case for reactive mass oral cholera vaccinations. *PLoS Neglected Tropical Diseases*, 5(1), e952. https://doi.org/10.1371/journal.pntd.0000952

[20] Routh, E. J. (1877). *A Treatise on the Stability of a Given State of Motion, Particularly Steady Motion*. Macmillan and Co.

[21] Sodjinou, V. D., Talisuna, A., Braka, F., Barboza, P., Alberti, K., Fortin, A., & Gueye, S. A. (2022). The 2021 cholera outbreak in West Africa: Epidemiology and public health implications. *Archives of Clinical and Biomedical Research*, 6(2), 296–307.

[22] Stoltzfus, J. D., Carter, J. Y., Akpinar-Elci, M., Matu, M., Kimotho, V., Giganti, M. J., & Elci, O. C. (2014). Interaction between climatic, environmental, and demographic factors on cholera outbreaks in Kenya. *Infectious Diseases of Poverty*, 3, 1–9. https://doi.org/10.1186/2049-9957-3-2

[23] Wang, J. (2022). Mathematical models for cholera dynamics—A review. *Microorganisms*, 10(12), 2358. https://doi.org/10.3390/microorganisms10122358

[24] World Health Organization. (2023). *Cholera annual report fact sheet*. https://www.who.int/news-room/fact-sheets/detail/cholera

[25] Wang, X., & Wang, J. (2016). Analysis of cholera epidemics with bacterial growth and spatial movement. *Journal of Biological Dynamics*, 10(1), 233–261. https://doi.org/10.1080/17513758.2016.1173650

[26] World Health Organization. (2023). *Cholera: Key facts*. https://www.who.int/news-room/fact-sheets/detail/cholera

[27] Zhou, X. Y., & Cui, J. A. (2013). Threshold dynamics for a cholera epidemic model with periodic transmission rate. *Applied Mathematical Modelling*, 37(5), 3093–3101. https://doi.org/10.1016/j.apm.2012.07.038

©*Simiyu et al. 2026.; This is an Open Access article distributed under the terms of the Creative Commons Attribution License http://creativecommons.org/licenses/by/4.0, which permits unrestricted use, distribution, and reproduction in any medium, provided the original work is properly cited.*

Licensed Under Creative Commons Attribution (CC BY-NC)